Journal of Colloid and Interface Science **256,** 325–330 (2002)
doi:10.1006/jcis.2002.8669

Fluorescent Hard-Sphere Polymer Colloids for Confocal Microscopy

Andrew I. Campbell and Paul Bartlett[1]

School of Chemistry, University of Bristol, Bristol BS8 1TS, United Kingdom

Received April 8, 2002; accepted August 14, 2002

We describe a single-stage synthesis of fluorescent hard-sphere polymer colloids. Monodisperse sterically stabilized poly(methyl methacrylate) spheres were prepared by a dispersion copolymerization of methyl methacrylate and methacrylic acid in the presence of a nonpolymerizable dye. The PMMA colloids are intensely fluorescent and when dispersed in hydrocarbons interact as classical hard spheres. At high concentrations they rapidly nucleate highly ordered three-dimensional colloidal crystals. Four different fluorophores were investigated to minimize the degree of fluorescence photobleaching at $\lambda = 488$ nm. The dye, 1,1′-dioctadecyl-3,3,3′,3′-tetramethylindocarbocyanine perchlorate ($DiIC_{18}$), was observed to photobleach at a significantly slower rate than existing materials (Bosma *et al.*, *J. Colloid Interface Sci.* 245, 292 (2002); Jardine and Bartlett, *Colloid Surf. A*, in press). We show the usefulness of the resulting $DiIC_{18}$ particles for confocal investigations of colloidal phenomena.

Key Words: **Polymer latices; dispersion polymerization; fluorescence; confocal microscopy; hard spheres.**

1. INTRODUCTION

Because of their large size and slow time scales, monodisperse colloids are probably one of the most widely studied models of soft condensed matter (1). For many years, the microscopic structure of suspensions has been studied using scattering methods. While scattering techniques have provided valuable insights into many fundamental colloidal problems, they do have limitations. For instance, investigations of the structure and dynamics of dense amorphous phases such as colloidal gels are difficult. The problem is that scattering probes Fourier components of the fluctuations in the particle density rather than the real-space density. Consequently, interpretation of scattering data requires a structural model, which is not always available. One promising approach to circumventing these problems is to image the bulk microscopic structure directly using three-dimensional fluorescence confocal microscopy. When combined with sophisticated particle tracking algorithms, confocal microscopy can yield the three-dimensional coordinates of upward of 10^4 particles with a high degree of accuracy (2–5). The resulting list of particle coordinates may then be used to characterize the detailed structure and dynamics of the colloidal phase.

The first applications of confocal microscopy to dense colloidal systems employed particles with a fluorescent core surrounded by a thick (∼300 nm) nonfluorescent shell (6). While the particles were visible due to the fluorescent core, they remained optically separated because of the thick nonfluorescent shell of material between touching spheres. Consequently, the centers of individual particles could be easily located. Although elegant, this approach relies upon the availability of suitable core–shell particles. While a number of synthetic methods have been described to prepare fluorescent core–shell particles (for an overview see Ref. (7)), they are all relatively complex multistep procedures. The situation was significantly improved when Dinsmore *et al.* (5) detailed how the use of sophisticated image analysis algorithms enables the three-dimensional coordinates of touching *volume-labeled* spheres to be determined from confocal microscopy. The algorithms used, however, place stringent requirements on the colloidal system. In particular, the colloidal spheres should show minimal photobleaching and be near-monodisperse in size. These two conditions need to be further supplemented if the particles are intended to provide a model system by the requirement that the particle potential should be hard-sphere-like. In addition, if the particles are to be refractive index or density matched, they must also be stable in a range of nonaqueous solvents.

There have been a number of recent attempts to synthesize polymer colloids that fulfill these requirements. Dinsmore *et al.* dyed poly(methyl methacrylate) spheres using an organic solvent to swell and transport dye into the particle core (5). Experiments showed that the resulting particles, when suspended in cycloheptyl bromide, were charged. In an alternate approach, Bosma *et al.* (8) and Jardine and Bartlett (9) described the preparation of labeled PMMA spheres by copolymerization of methyl methacrylate with the reactive methacryloylated dye, 4-methylaminoethylmethacrylate-7-nitrobenzo-2-oxa-1,3-diazol (NBD). The NBD-dyed particles were uniform in size and, in at least some situations, showed hard-sphere interactions (9). Unfortunately, the synthesis of the methacryloylated dye is an elaborate time-consuming procedure and furthermore the NBD chromophore is not ideal for quantitative confocal studies because the dye rapidly photobleaches. Because of these limitations, it would be useful to have a method which was simpler

[1] To whom correspondence should be addressed. E-mail: P.Bartlett@bristol.ac.uk.

0021-9797/02 $35.00

and at the same time versatile enough to allow the chromophore to be varied in an effort to minimize photobleaching. Here, we report a straightforward single-pot procedure for the preparation of large monodisperse fluorescent polymer particles suitable for confocal microscopy in which the particles are dyed *in situ* during the polymerization process. Incorporation of dye can be performed much easier than the existing procedures. Dye-impregnated particles are monodisperse and interact as hard spheres. By careful selection of dye, we reduce substantially the extent of photobleaching in comparision with NBD-labeled spheres. The resulting dyed particles are ideally suited to quantitative confocal studies.

2. MATERIALS AND METHODS

Synthesis. The dyes 1,1′-dioctadecyl-3,3,3′,3′-tetramethylindocarbocyanine perchlorate ($DiIC_{18}$, Fluka), 3,3′-dioctadecyloxacarbocyanine perchlorate ($DiOC_{18}$, Sigma), 9-diethylamino-5*H*-benzo[α]phenoxazine-5-one (Nile Red, Aldrich), and 3,6-bis(dimethylamino) acridine hydrochloride (Acridine Orange, Aldrich) were used as received (Fig. 1). The dispersion polymerization was modified from the procedure described by Antl *et al.* (10). In a typical example, 0.27 g of α,α'-azo-bis-isobutyronitrile (Acros), 8.3 mg of the dye $DiIC_{18}$, and 0.18 g of octanethiol (Aldrich) were dissolved at room temperature in a mixture of 34.4 g of methyl methacrylate and 0.71 g of methacrylic acid (both from Aldrich) in a 250-ml round-bottomed flask equipped with a reflux condenser. Prior to use, the inhibitor was removed from the monomers by a column of activated aluminum oxide. A solution of 1.76 g of the polymeric poly(12-hydroxy stearic acid) graft copolymer stabilizer (PHSA), synthesized following the multistep procedure detailed in Ref. (10), 15.8 g of hexane, and 7.9 g of dodecane was added and the polymerization started by placing the reaction mixture in an thermostated oil bath at 80°C. The reaction was continued for 2 h to ensure complete reaction of the monomers. The stabilizer was covalently attached to the surface of the particles by the addition of 15.8 g of dodecane and 0.15 g of 2-dimethylaminoethanol (Acros) and the mixture refluxed at 120°C for an additional 24 h.

The reaction product was diluted with dodecane and filtered through glass wool to remove coagulum. Excess stabilizer and dye were removed by centrifugation (60 min at 15,000 rpm), the supernatant was decanted, and the colloid was redispersed in clean dodecane. The procedure was repeated, typically eight times, until the dye was no longer detectable in the supernatant.

Characterization. The diameter (d) and polydispersity (σ) of the particles were determined by static light scattering (SLS) and electron microscopy (JEOL JSM-6310). SLS measurements were performed on dilute dispersions in *cis*-decalin (Avocado) using a homemade apparatus. The suspension was diluted until the number-corrected particle intensity became independent of dilution. The wavelength of the incident radiation was 488 nm. To suppress fluorescence, an interference filter was placed in front of the photodetector. The measured intensity profile was fitted by nonlinear regression to a polydisperse form factor calculated assuming a homogeneous refractive index profile.

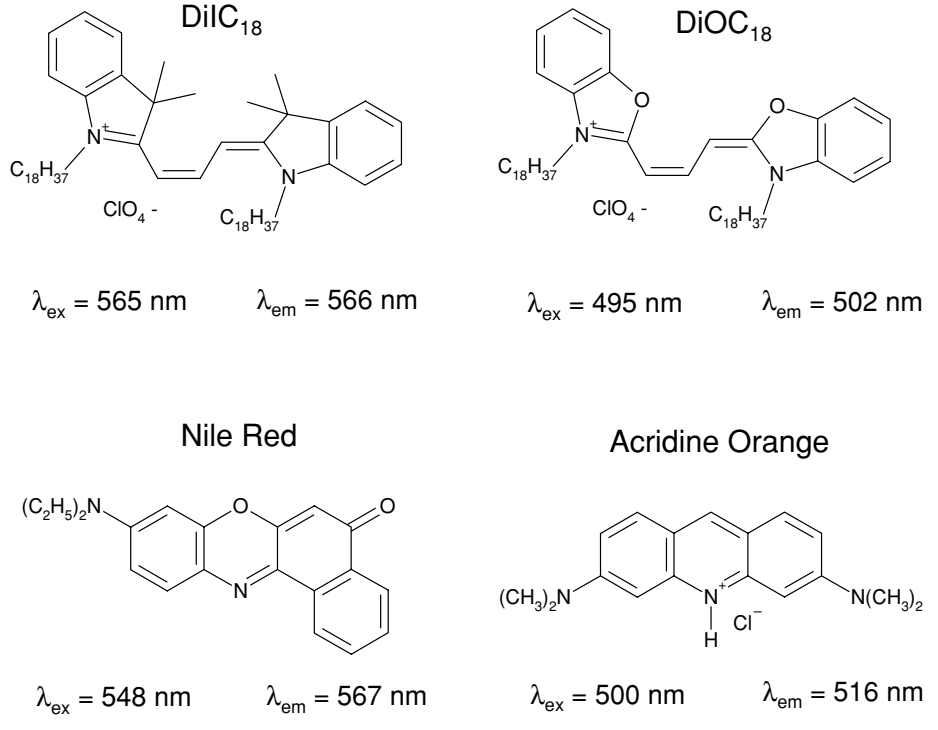

FIG. 1. Fluorescent dyes and their excitation and emission maxima when incorporated into PMMA colloids.

The density of the latex was found using a mixture of *cis*-decalin ($\rho = 0.897$ g cm^{-3}) and cycloheptyl bromide (CHB; $\rho = 1.289$ g cm^{-3}). Dilute suspensions ($\phi = 0.02$) were spun in a centrifuge at 90g and the sedimentation velocity was recorded. The mass density of the neutrally buoyant solvent mixture was determined as 1.166 g cm^{-3} and corresponded to a *cis*-decalin mass fraction of $m = 0.241$.

The location of the fluid–solid phase transition was determined in a *cis*-decalin/CHB mixture ($m = 0.301$). The dispersions were concentrated by centrifugation (90g for 2 h) and a weighed amount of the supernatant was removed to create samples with concentrations which spanned the anticipated freezing and melting transitions. The samples were sealed carefully, left to stand, and observed visually for 30 days. The crystalline fraction was recorded as a function of time and corrected for gravitational sedimentation following the procedure described by Paulin and Ackerson (11).

Fluorescence emission and excitation spectra were recorded on a Perkin-Elmer LS50B spectrometer. To minimize scattering, the particles were refractive index matched. The emission spectrum was recorded by illumination at the maximum of the corresponding excitation spectrum.

Confocal microscopy. Samples for confocal microscopy (Carl Zeiss LSM-Pascal) were made by dispersing labeled particles in a refractive index matched mixture of *cis*-decalin and CHB. The CHB was distilled under a reduced pressure at 75°C immediately prior to use. The suspensions were sealed in glass capillaries 0.1-mm thick (Vitrocom, USA) and imaged with a 1.4 NA/63× oil-immersion objective using either an argon-ion ($\lambda = 488$ nm) or He–Ne laser ($\lambda = 543$ nm) for excitation. The rate of photobleaching was measured by scanning repeatedly a two-dimensional layer of particles using a fixed intensity laser. Each pixel corresponded to a sample area of 0.29×0.29 μm^2. The total image intensity was evaluated and plotted as a function of the laser illumination time per pixel.

3. RESULTS AND DISCUSSION

Particle preparation. Monodisperse, dyed PMMA spheres with sizes between 1.0 and 2.4 μm were synthesized using the recipes listed in Table 1. Nonpolymerizable fluorescent dyes were incorporated by dissolving the dye in the monomer prior to polymerization. Dispersion polymerization is very sensitive to the polarity of the dispersion medium, the concentrations of monomers and initiator, and the type and level of steric stabilizer (12). The relationship between these variables is complex and the reaction conditions need to be finely tuned to produce stable monodisperse polymer particles. Previous work (13) has shown that the presence of a dye can have a significant deleterious effect on a free-radical polymerization. For instance, of the eight dyes added by Horak *et al.* (13) to a dispersion polymerization of styrene, only one dye did not interfere with particle formation. The other remaining dyes significantly inhibited the progress of the free-radical polymerization, causing high degrees of particle polydispersity and low rates of monomer conversion. A key consideration in selecting favorable dyes is that all the reactants need to be soluble in the reaction medium at the beginning of the polymerization. This requirement poses some difficulties because the majority of fluorescent dyes have unsuitable solubility characteristics. Our best results were obtained when we used octadecyl-substituted carbocyanine dyes, commonly used as probes of lipophilic membrane structure (14). Figure 1 details the chemical structures of the dyes studied together with the maxima of their excitation and emission spectra when incorporated into PMMA. The dyes (apart from Nile Red) are only partially soluble in hydrocarbons and, consequently, readily partition into the more polar PMMA phase. Once incorporated, the dye is physically entrapped as a result of the high-T_g of the PMMA matrix. To prove that the dye was immobilized, we tried to extract the dye by repeatedly washing the colloid with decane. The PMMA–NR latex was centrifuged, the supernatant collected and analyzed, and the colloid then redispersed in clean decane. This procedure was repeated daily for 2 weeks. The concentration of dye in the supernatant dropped rapidly with time, becoming essentially undetectable after ~5 days. Since the latex remained brightly colored, we interprete the observation as indicating the initial fluorescence of the supernatant that originated from free dye in the suspension rather than the leaching of dye out of the particles.

TABLE 1
Properties of Dyed PMMA Colloids

System	Monomer (wt%)	$d \pm 0.05$ (μm)	$\sigma \pm 0.01$	Dye conc. (10^{-2} wt%)	Dye incorporated
PMMA–DiIC$_{18}$(a)	53.97	1.08	0.05	1.28	DiIC$_{18}$
PMMA–NR	54.04	1.30	0.07	1.00	Nile Red
PMMA–DiIC$_{18}$(b)	54.98	1.55	0.03	1.32	DiIC$_{18}$
PMMA–AO	55.96	1.59	0.21	2.40	Acridine orange
PMMA–DiOC$_{18}$	56.00	1.84	0.05	0.69	DiOC$_{18}$
PMMA–DiIC$_{18}$(c)	57.99	2.40	0.05	1.31	DiIC$_{18}$

Note. The proportions of monomer and dye are given as a weight percentage of the reaction mixture.

Figure 2 shows a SEM micrograph of the synthesized dyed PMMA particles. The particles are spherical and monodisperse with a polydispersity ratio $\sigma = \sqrt{\langle R^2\rangle/\langle R\rangle^2 - 1}$ of ~0.03. Using three of the four dyes, it was possible to obtain near-monodisperse polymer particles. Incorporation of acridine orange was least successful with polydispersity levels rising to $\sigma = 0.21$. In contrast to Ref. (13) we observed relatively minor changes in the rate of polymerization in the presence of the dye. This probably reflects the low concentration of dye needed for fluorescent labeling (here ~10^{-2} wt%) in comparison with the significantly higher dye concentrations required for absorption labeling (~10^{-1} wt% (13)).

Photobleaching. The tendency for fluorescent dyes to photobleach after prolonged laser excitation is a serious limitation

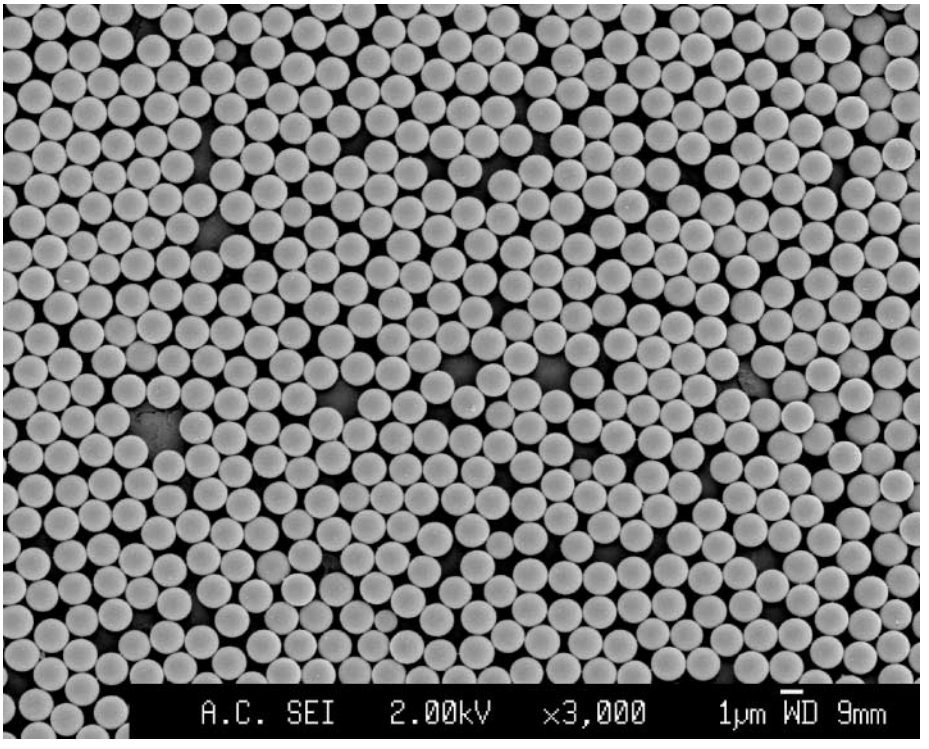

FIG. 2. SEM image of the PMMA–DiIC$_{18}$(b) particles.

in quantitative confocal microscopy (15). Rapid photobleaching changes the image intensity with time, significantly complicating image analysis. While all fluorescent dyes photobleach to some extent, the rapidity of bleaching depends sensitively upon the dye's electronic structure, its environment, the laser wavelength, and intensity. Ideally, the dye should photobleach sufficiently slowly that there would be no significant change in fluorescent intensity during the time required to collect an 3D-image stack ($\sim$1 min). To determine the extent of photobleaching, we measured the fluorescent yield under conditions of identical pixel size, laser intensity, and wavelength λ. The fluorescence decay at $\lambda = 488$ nm is plotted in Fig. 3 where it is compared with similar measurements on NBD-labeled spheres (9). Significant variations in the rate of bleaching are clearly evident. The decay of the fluorescent yield with time is not well described, in general, by a single-exponential function. Consequently, to compare the photobleaching characteristics of the differently labeled particles, we determined the time taken (τ_{70}) for the fluorescence intensity to drop to 70% of its original value. In terms of this time the PMMA–DiIC$_{18}$ particles bleach in excess of 30 times slower ($\tau_{70} = 7.8$ ms) than the NBD-labeled PMMA spheres ($\tau_{70} = 0.23$ ms). A similar trend was found at $\lambda = 543$ nm with again the dialkylcarbocyanine-labeled particles the most resistant to photobleaching (data not shown).

Interparticle interactions. To ascertain if the dyed colloids are suitable as model systems, we determined the position of the fluid–crystal phase boundary. As an example, we show in Fig. 4 the equilibrium phase diagram for PMMA–DiIC$_{18}$ particles with a diameter of 1.55 μm. The volume fraction of the particle cores ϕ_c (excluding the stabilizer layer) was obtained from the colloid mass and the PMMA–DiIC$_{18}$ particle density. The corresponding freezing and melting densities were determined as $\phi_c^f = 0.468$ and $\phi_c^m = 0.510$. Assuming that the effective volume fraction (including the stabilizer layer) at freezing

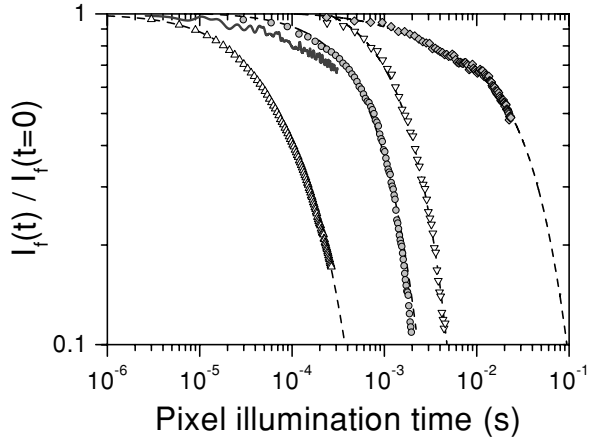

FIG. 3. Photobleaching characteristics of PMMA particles at $\lambda = 488$ nm. The fluorescence intensity is plotted as a function of the laser illumination time per pixel (△ PMMA–A0, ● PMMA–DiOC$_{18}$, ▽ PMMA–NR, ◆ PMMA–DiIC$_{18}$(c)). The solid line depicts data for the PMMA–NBD system from (9). The dashed lines are multiexponential fits to the data.

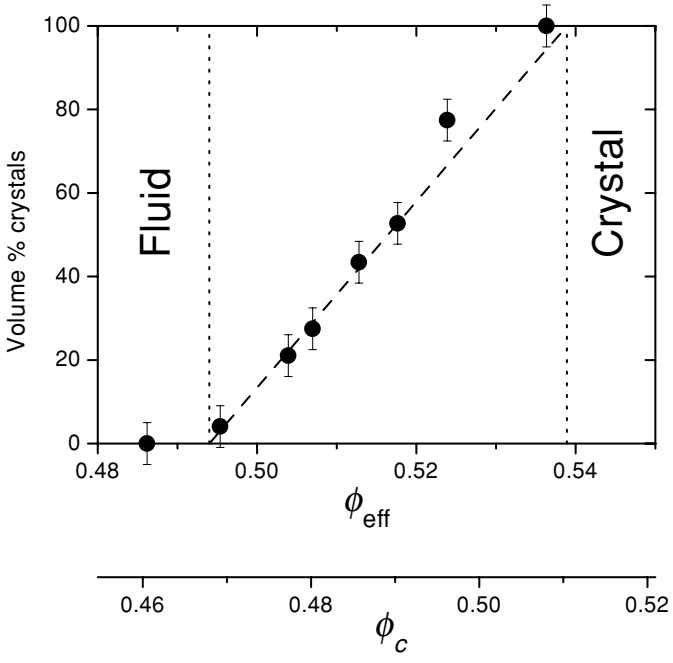

FIG. 4. The fluid–crystal phase diagram measured in the system PMMA–$DiIC_{18}$ (b). The observed percentage of crystal is plotted as a function of the core volume fraction (ϕ_c) and the equivalent effective hard-sphere volume fraction ϕ_{eff}. The dashed lines label the positions of the freezing and melting transitions. The melting transition at $\phi^m_{eff} = 0.539$ is in close agreement with the value expected for hard spheres, $\phi^m = 0.545$.

is $\phi^f_{eff} = 0.494$ (16), we estimate the thickness of the stabilizer layer as 14 nm, close to the value expected for an extended PHSA chain (~10 nm). This confirms that the repulsive interactions between particles are short-ranged. In particular, there is no electrostatic contribution to the potential, as has been seen in related systems (5). The corresponding melting volume fraction $\phi^m_{eff} = 0.539$ is in excellent agreement with hard-sphere simulations ($\phi^m = 0.545$) (17) which since this transition depends sensitively on the interparticle interactions confirms that the dyed particles interact essentially as hard spheres.

Confocal microscopy confirmed the nature of the interaction potential. Figure 5a shows a single confocal image of PMMA–$DiIC_{18}$ particles (1.55 μm in diameter) dispersed in a mixture of 66% CHB and 34% *cis*-decalin (by weight). The suspension volume fraction ($\phi_{eff} = 0.513$) was within the two-phase region and a colloidal crystal formed rapidly. The three-dimensional structure was studied by collecting a stack of 100 images, separated vertically by 0.16 μm. The total volume imaged was 91.4 μm × 91.4 μm × 15.8 μm and contained particles arranged in 11 vertically stacked close-packed planes. To quantify the translational order, we calculated the two-dimensional radial distribution function (rdf) $g_{2D}(r)$ from the confocal images using image analysis to identify the 3D centers of each particle. Figure 5b shows the averaged in-plane rdf, $g_{2D}(r)$. The first peak in $g_{2D}(r)$ corresponds to the average separation between nearest-neighboring spheres within a hexagonally packed plane of spheres. This spacing is equal to the 2D-hexagonal lattice constant a which, since the spheres are not close packed, exceeds the particle diameter d. For a hexagonal planar net of spheres $g_{2D}(r)$ contains peaks at 1, $\sqrt{3}$, 2, $\sqrt{7}$, 3, $2\sqrt{3}$, $\sqrt{13}$, 4, $\sqrt{19}$, $\sqrt{21}$, and 5 (in units of a). Indexing in this way, the peaks in Fig. 5b, gave a lattice constant $a = 1724$ nm. In a close-packed crystal the hexagonal planes are stacked along the c-axis with a spacing of $\sqrt{2/3}a$. If the particles behave as hard spheres, then the crystal volume fraction ϕ is simply $\phi = \pi\sqrt{2}d^3/6a^3$ with d the particle diameter. Taking the crystal volume fraction as

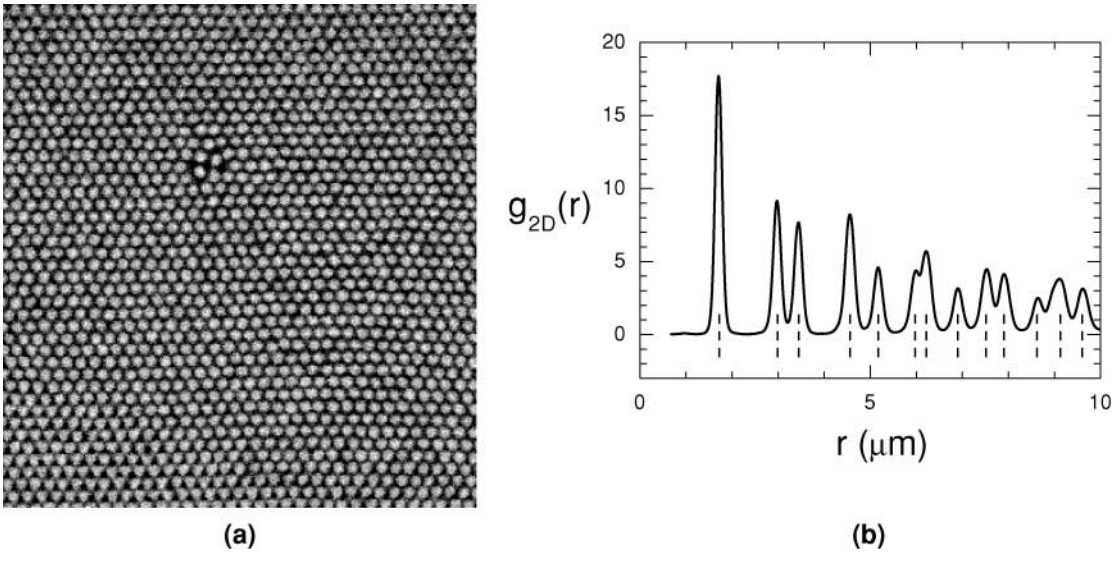

FIG. 5. (a) Confocal image of a crystalline array of PMMA–$DiIC_{18}$(b) particles (diameter 1.55 μm). (b) Two-dimensional radial distribution function $g_{2D}(r)$. The dashed lines indicate the positions of the nearest neighbors for a two-dimensional hexagonal lattice with a unit cell size $a = 1724$ nm.

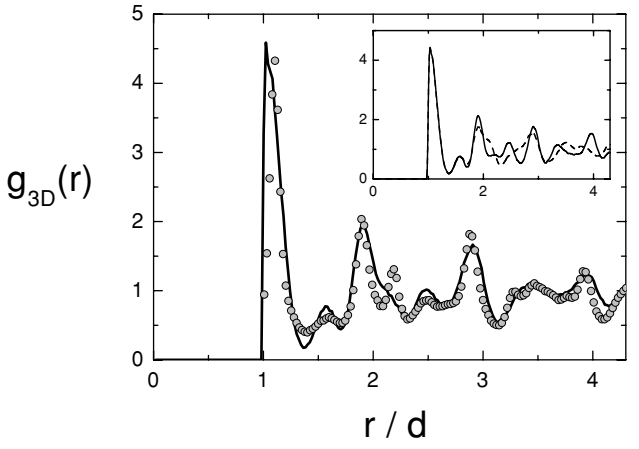

FIG. 6. Three-dimensional radial distribution function, $g_{3D}(r)$, of the crystalline phase formed in a suspension of PMMA–DiIC$_{18}$(b) particles ($\phi_{\text{eff}} = 0.513$). The sample lies within the region of fluid–crystal coexistence (see Fig. 4). The solid line depicts the radial distribution function calculated for a purely random-stacked crystal of hard spheres, at melting ($\phi = 0.55$). The close agreement shows the hard-sphere character of the dyed PMMA spheres. The inset diagram illustrates the differences between the radial distribution functions calculated for a fcc (solid) and a hcp (dashed) hard-sphere crystal at $\phi = 0.55$.

$\phi = 0.545$ yields a diameter of 1.56 μm, which is in excellent agreement with light scattering and electron microscopy (see Table 1).

The three-dimensional structure of the crystals were characterized by identifying the central coordinates of 34,012 individual particles from consecutive confocal images. The particle positions were determined numerically by a home-written suite of image analysis routines (based, in part, on algorithms published by Crocker and Grier (18)). These routines work efficiently as a result of the photostability and high levels of monodispersity of the PMMA–DiIC$_{18}$ particles. Although an extensive analysis of the crystal structure has yet to be performed, we show in Fig. 6 the corresponding *three-dimensional* radial distribution function, $g_{3D}(r)$. While the measured $g_{3D}(r)$ has many features in common with the hard-sphere rdf computed by simulation (19) for the face-centered cubic and hexagonal close-packed crystalline phases, we were unable to accurately reproduce the experimental data by either phase alone. Previous experimental work (20) has indicated that hard spheres form random-stacked structures in which the plane stacking sequence is intermediate between pure fcc and hcp phases. To test for this possibility, we simulated the rdf of the random-stacked crystal by Monte Carlo techniques. Figure 6 shows a comparison between the radial distribution function calculated assuming a random-stacked crystal (full line) and the experimental data (shown as points). While the agreement is not perfect, the comparison is convincing and indicates that the crystal formed has indeed a structure intermediate between fcc and hcp, as expected for a system of hard spheres.

4. CONCLUSIONS

We have described a straightforward procedure for the synthesis of fluorescent hard-sphere colloids. The preparation is significantly easier than methods described recently (8, 9) and in addition allows a wider range of dyes to be incorporated. We have shown that by a careful selection of fluorophore, it is possible to reduce significantly the extent of photobleaching. Characterization of the interparticle potential by phase equilibria and confocal microscopy shows that the dyed particles interact as classical hard spheres. The fluorescent hard-sphere particles described here should be useful as a model for future confocal investigations.

ACKNOWLEDGMENTS

We thank Dr. V. Anderson for the simulation of the radial distribution function and M. Iles for phase equilibria measurements. Financial support from the UK Engineering and Physical Sciences Research Council and Aventis, for the award of a CASE studentship to AIC, is gratefully acknowledged.

REFERENCES

1. Pusey, P. N., *in* "Liquids, Freezing and Glass Transition" (J. P. Hansen, D. Levesque, and J. Zinn-Justin, Eds.), NATO Advanced Study Institute at Les Houches, Session LI, 3–28 July 1989, pp. 763–942. North Holland, Amsterdam, 1991.
2. Van Blaaderen, A., and Wiltzius, P., *Science* **270,** 1177 (1995).
3. Weeks, E. R., Crocker, J. C., Levitt, A. C., Schofield, A., and Weitz, D. A., *Science* **287,** 627 (2000).
4. Gasser, U., Weeks, E. R., Schofield, A., Pusey, P. N., and Weitz, D. A., *Science* **292,** 258 (2001).
5. Dinsmore, A. D., Weeks, E. R., Prasad, V., Levitt, A. C., and Weitz, D. A., *Appl. Opt.* **40,** 4152 (2001).
6. Blaaderen, A., Imhof, A., Hage, W., and Vrij, A., *Langmuir* **8,** 1514 (1992).
7. Schartl, W., *Adv. Mater.* **12,** 1899 (2000).
8. Bosma, G., Pathmamanoharan, C., de Hoog, E. H., Kegel, W. K., van Blaaderen, A., and Lekkerkerker, H. N. W., *J. Colloid Interface Sci.* **245,** 292 (2002).
9. Jardine, R., and Bartlett, P., *Colloid Surf. A*, in press.
10. Antl, L., Goodwin, J. W., Hill, R. D., Ottewill, R. H., Owens, S. M., Papworth, S., and Waters, J. A., *Colloid Surf.* **17,** 67 (1986).
11. Paulin, S. E. and Ackerson, B. J., *Phys. Rev. Lett.* **64,** 2663 (1990).
12. Croucher, M. D., and Winnik, M. A., *in* "Scientific methods for the study of polymer colloids and their applications" (F. Candau and R. H. Ottewill, Eds.), pp. 35–72. Kluwer, Amsterdam, 1990.
13. Horak, D., Svec, F., and Frechet, J. M. J., *J. Polym. Sci. A* **33,** 2961 (1995).
14. Haughland, R., "Handbook of Fluorescent Probes and Research Chemicals." Molecular Probes, Inc., Eugene, OR, 1996.
15. Pawley, J. B., "Handbook of Biological Confocal Microscopy," 2nd ed. Plenum, New York, 1995.
16. Pusey, P. N., and van Megen, W., *Nature* **320,** 340 (1986).
17. Hoover, W. G., and Ree, F. H., *J. Chem. Phys.* **49,** 3609 (1968).
18. Crocker, J. C., and Grier, D. G., *J. Colloid Interface Sci.* **179,** 298 (1996).
19. Choi, Y. M., Ree, T., and Ree, F. H., *J. Chem. Phys.* **95,** 7548 (1991).
20. Pusey, P. N., van Megen, W., Bartlett, P., Ackerson, B. J., Rarity, J. G., and Underwood, S. M., *Phys. Rev. Lett.* **63,** 2753 (1989).